J Mater Sci (2011) 46:5278–5281
DOI 10.1007/s10853-011-5466-z

Yttrium-doped effect on thermoelectric properties of $La_{0.1}Sr_{0.9}TiO_3$ ceramics

Y. Sun · C. L. Wang · H. C. Wang · H. Peng · F. Q. Guo · W. B. Su · J. Liu · J. C. Li · L. M. Mei

Received: 7 November 2010 / Accepted: 11 March 2011 / Published online: 23 March 2011

Abstract Ceramic samples of $La_{0.1}Y_xSr_{0.9-x}TiO_3$ with different yttrium concentration have been synthesized by conventional solid state reaction technique, and their thermoelectric properties have been investigated. X-ray diffraction characterization confirms that the main crystal structure is of perovskite, but with a small amount of second phase of $Y_2Ti_2O_7$ for samples with $x = 0.05$, 0.08, and 0.10. SEM images indicate all ceramic samples are dense and compact, and the largest grain size appears in sample with $x = 0.03$ and 0.05. Also the second phase can also be identified from the SEM images for $x = 0.05$, 0.08, and 0.10 samples. Electrical conductivity and Seebeck coefficient of samples have been measured in the temperature range between 300 and 1100 K. With increasing of yttrium concentration, electrical resistivity decreases, and reaches 0.8 mΩ cm for $x = 0.10$ sample at room temperature. The absolute Seebeck coefficients increase monotonically with increasing temperature in the whole temperature range. Sample with $x = 0.03$ exhibits the highest absolute Seebeck coefficient 219 μV K^{-1} at 1059 K, as well as the maximum power factor 11 μW cm^{-1} K^{-2} at 624 K.

Y. Sun (✉) · C. L. Wang · H. C. Wang · H. Peng · W. B. Su · J. Liu · J. C. Li · L. M. Mei
School of Physics, State Key Laboratory of Crystal Materials, Shandong University, Jinan 250100, Peoples of Republic China
e-mail: gghels@163.com

Y. Sun · F. Q. Guo
Department of Physics, Changji University, Xinjiang Uyghur Autonomous Region, Changji 830100, Peoples of Republic China

Introduction

Thermoelectric materials with high-energy conversion efficiency are strongly required for both the refrigeration of electronic devices and electric power generation in terms of waste heat recovery. The thermoelectric performance is essentially evaluated by the dimensionless figure of merit $ZT = S^2T/\rho\kappa$, where T, S, ρ, and κ represent absolute temperature, Seebeck coefficient, electrical resistivity, and thermal conductivity, respectively. To increase the thermoelectric performance, materials should have lower κ, and high-power factor S^2/ρ. Because of the relatively low carrier mobility of oxides, they were generally not recognized as good thermoelectric materials [1]. However, oxides do have so many advantages to serve as thermoelectric materials, such as non-toxic, low-cost, and good thermal stability, etc. Oxides thermoelectric materials have received much attention [2–13] since the report of high-thermoelectric performance in $NaCo_2O_4$, which shows a large Seebeck coefficient (about 100 μV K^{-1} at 300 K) and a relatively high conductivity around 2×10^4 Scm^{-1} at room temperature [2]. Though some *p*-type cobalt oxides exhibit a large figure of merit (*ZT*) that is comparable to conventional alloys materials [3, 5, 10], *n*-type oxide thermoelectric materials with high thermoelectric performance are inevitably expected as a counter-partner of the *p*-type oxide materials for constructions of thermoelectric modules. Different elements doped $SrTiO_3$ has been reported as a potential candidate for *n*-type thermoelectric oxides with a high-power factor. Okuda et al. [4] reported that La-doped $SrTiO_3$ single crystal shows high-power factor at room temperature, 28–36 μW cm^{-1} K^{-2}, which is comparable to Bi_2Te_3 alloys. Ohta et al. [9] reported that of properties Nb-doped $SrTiO_3$ epitaxial film. A relatively high-power factor about 1.5×10^{-3} Wm^{-1} K^{-2} has been

obtained, which is approximately half of practically used SiGe alloys, and the figure of merit ZT for $SrTi_{0.8}Nb_{0.2}O_3$ can be reached 0.37 at 1000 K. Most recently, La-doped SrTiO3 thin film grown by molecular beam epitaxy has been investigated by Jalan et al. [14], a maximum power factor 39 μW cm^{-1} K^{-2} which is comparable to that of the single crystalline bulk $SrTiO_3$ was reported. Wang et al. [12] reported that figure of merit ZT of 0.36 has been obtained at 1045 K. Also, it was noticed that the electrical conductivity of Y-doped $SrTiO_3$ is much higher than that of La-doped $SrTiO_3$ [15]; and the power factor can be increased significantly in Y-doped $SrTiO_3$ [6, 7]. Encouraged by these results of above studies, influence of yttrium doping on the thermoelectric properties of $La_{0.1}Sr_{0.9}TiO_3$ ceramic is investigated in this study. Ceramic samples of $La_{0.1}Y_xSr_{0.9-x}TiO_3$ with $0 \leq x \leq 0.10$ have been prepared by the solid state reaction method. Their thermoelectric properties have been measured in temperature range between 300 and 1100 K, and the effects of yttrium doping on thermoelectric properties of $La_{0.1}Sr_{0.9}TiO_3$ ceramic have been discussed.

Experimental

Ceramic samples of $La_{0.1}Y_xSr_{0.9-x}TiO_3$ with $x = 0.01$, 0.03, 0.05, 0.08, and 0.10 were prepared by conventional solid state reaction techniques. The starting materials were La_2O_3 with a purity of 99.99%, $SrCO_3$ with a purity of 99%, TiO_2 with a purity of 99.8%, and Y_2O_3 with a purity of 99.5%. These raw materials were weighed in stoichiometric proportions, and mixed by ball-milling in ethanol with zirconia balls for 12 h. After the wet mixtures dried, they were pressed into pellets, and calcined at 1350 °C for 6 h in air. The pellets were smashed and ball-milled for 12 h to obtain a fine powder. Then the powder was repressed into pellets. These pellets were sintered at 1460 °C for 4 h to forming gas with 5 mol% hydrogen in argon. The sintered pellets were cut into rectangular columns with dimensions of 20 × 1.8 × 1.8 mm^3 to measure the thermoelectric properties. These columns were coated with four electrodes, two on each ends and two on sides, with silver paint annealed at 850 °C for 30 min. For electric measurements, four-probe method was used in the measurement of electrical resistivity ρ. A direct current I of 100 mA was set to pass through the two end electrodes and the potential difference V across the two side electrodes was read. For measurement of Seebeck coefficient S, two NiCr–NiSi thermal couples were attached on each side electrodes of the column with a separation of 8.0 mm. A temperature difference $\Delta T = T_2 - T_1$ about 3 °C was built up between the two thermal couples using an auxiliary heater during thermoelectric measurement. Seebeck coefficient S was determined from the slope of ΔV versus ΔT relation by the least-square method, where ΔV is the thermoelectromotive force produced by ΔT between the two electrodes. The crystal structure and lattice parameter were characterized by power X-ray diffraction with Cu $K\alpha$ radiation ($\lambda = 0.154056$ nm) utilizing a Bruker AXS D8 ADVANCE diffractometer. The surface morphology was obtained on a Hitachi S-4800 scanning electronic microscope (SEM).

Results and discussion

XRD patterns of $La_{0.1}Y_xSr_{0.9-x}TiO_3$ powders are shown in Fig. 1. The major diffraction peaks can be indexed with the cubic perovskite structure belonging to the $Pm\bar{3}m$space group. Light-doped sample $La_{0.1}Y_{0.01}Sr_{0.89}TiO_3$ and $La_{0.1}Y_{0.03}Sr_{0.87}TiO_3$ are of single phase in cubic structure. A second phase can be easily identified in samples of $x = 0.05$, 0.08, and 0.10. The diffraction intensity of the second phase also increases with yttrium content increasing. According to PDF card of no. 42-0413, the second phase is $Y_2Ti_2O_7$. Because the precise amount of the second phase is difficult to determine, the lattice parameters and theoretical densities were calculated using the lattice constants from XRD, and listed in Table 1. The variation of the values is very small and could be within the resolution limit of powder XRD. The theoretical density of the sintered samples is calculated from the lattice constants. The relative density is defined as measured density over the theoretical density, and the values are 96, 97, 96, 97, and 96% for $x = 0.01$, 0.03, 0.05, 0.08, and 0.10, respectively.

Scanning electronic microscope (SEM) images of surface microstructures for $La_{0.1}Y_xSr_{0.9-x}TiO_3$ ceramics are shown in Fig. 2a–e, for sample of $x = 0.01$, 0.03, 0.05, 0.08, and 0.10, respectively. All patterns show polygon morphology and compact. With the increasing yttrium

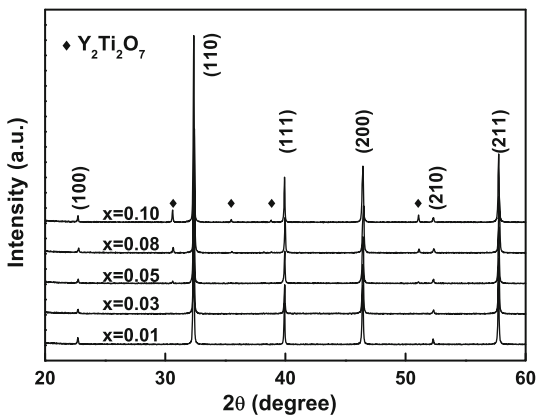

Fig. 1 X-ray diffraction patterns of $La_{0.1}Y_xSr_{0.9-x}TiO_3$ ($x = 0.01$, 0.03, 0.05, 0.08, and 0.10) powders

Table 1 Calculated lattice parameters, theoretical density, and relative density for $La_{0.1}Y_xSr_{0.9-x}TiO_3$ ceramics with $x = 0.01$, 0.03, 0.05, 0.08, and 0.10

x	a (Å)	V (Å^3)	Theoretical density (g/cm^3)	Relative density (%)
0.01	3.9079	59.68	5.257	96
0.03	3.9057	59.58	5.270	97
0.05	3.9055	59.57	5.262	96
0.08	3.9035	59.48	5.262	97
0.10	3.9064	59.61	5.254	96

concentration, average grain size is estimated as 2.8, 9.5, 13.2, 5.3, 3.3 μm, respectively. There exist fine grains without stripe patterns in Fig. 2c–e, which the authors believe they are the second phase ($Y_2Ti_2O_7$) in these ceramic samples, and $x = 0.03$ might be around the threshold quantity for emergence of the second phase.

Figure 3 shows the temperature dependence of electrical resistivity of $La_{0.1}Y_xSr_{0.9-x}TiO_3$ ceramics in temperature range between 300 and 1100 K. Three samples with $x = 0.03$, 0.08, and 0.10 are showing typical metallic behavior, their electrical resistivity increase with increasing temperature. The electrical resistivity for both $x = 0.01$ and 0.05 decrease with temperature increasing when temperature is below about 500 K, then increase with further increasing of temperature. This kind of semiconductive behavior coincides with the previous reports on polycrystalline samples [6, 11]. Electrical resistivity is determined by the carrier concentration and carrier mobility simultaneously. Y doped not only affects the carrier concentration, but also affects carrier mobility. Especially, the crystal grain size and amount of the second phase more influence carrier mobility. In $x = 0.01$ and 0.05 samples, when the temperature is below about 500 K, the carrier mobility is the dominant factor. Above 580 K, the electrical resistivity of all samples decreases with increasing of Y concentration. The electrical resistivity decrease from 6.8 mΩ cm for $x = 0.01$ at 1058 K to 5.5 mΩ cm for $x = 0.10$ at 1061 K. The electrical resistivity of $x = 0.10$ sample is nearly the same as that of $x = 0.08$ sample in the whole temperature range.

The temperature dependence of the Seebeck coefficient is shown in Fig. 4. All samples are showing negative Seebeck coefficients in the temperature range between 300 and 1100 K, indicating *n*-type conduction mechanism, or the main carriers are electrons. The absolute Seebeck coefficients of all samples increase monotonically with increasing temperature. Generally speaking, the absolute Seebeck coefficient decreases with the increasing yttrium concentration. This can be attributed to the carrier concentration increase with increasing of Y content [13]. However, the absolute Seebeck coefficient for $x = 0.03$ sample is the highest above 580 K. This may be ascribed to the second phase, even though they are small in size and few in number that hard to be detected in the sample. Accordingly to a recently report [12], the extreme value of property tend to be obtained in the critical point of second phase appearance. In the article, $x = 0.03$ may be the critical point of second phase emergence, so it tend to obtain the highest value of property as well. Yet, the mechanism of how the second phase would affect sample's electrical properties is not clear. Further research work should be done next.

Temperature dependence of the power factors, which is calculated from S^2/ρ, is presented in Fig. 5. With the increase of temperature, the power factor firstly increases and reaches a maximum around 600 K, then decrease with further increasing of temperature. The general trend of temperature dependence of the power factor does not changed by the Y concentration. The maximum values of power factor for $x = 0.01$, 0.03, 0.05, 0.08, and 0.10

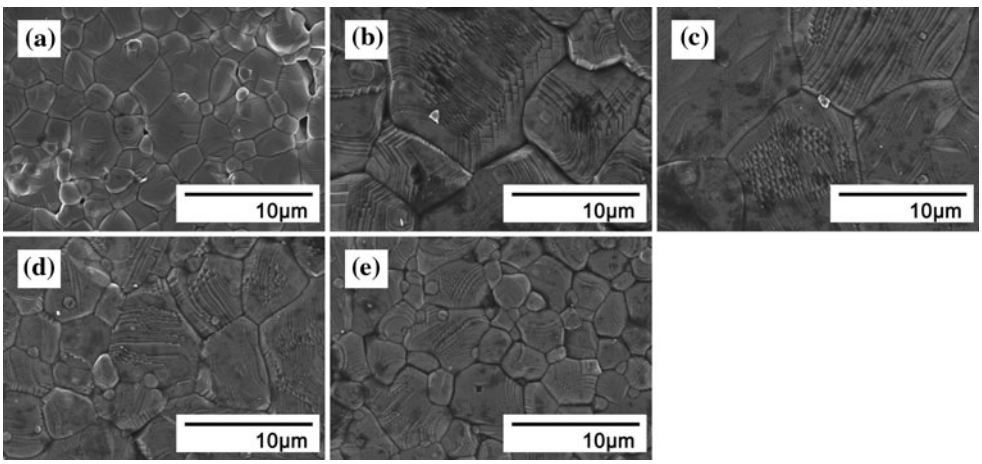

Fig. 2 SEM images of $La_{0.1}Y_xSr_{0.9-x}TiO_3$ ceramics (*a–e* represents $x = 0.01$, 0.03, 0.05, 0.08, and 0.10, respectively.)

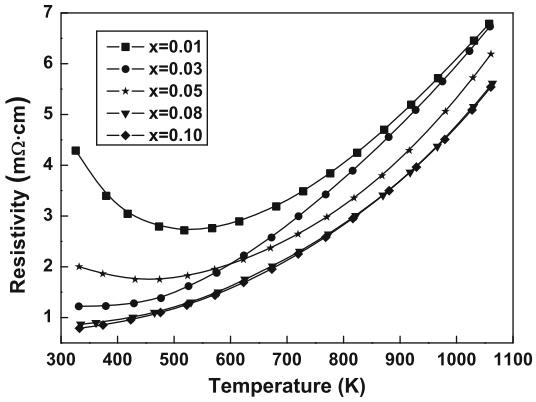

Fig. 3 Temperature dependence of electrical resistivity of $La_{0.1}Y_xSr_{0.9-x}TiO_3$ ($x = 0.01$, 0.03, 0.05, 0.08, and 0.10) ceramics

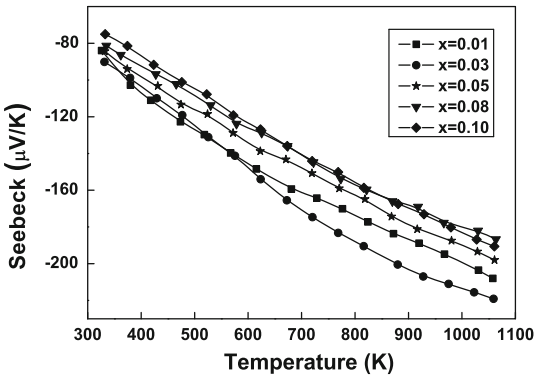

Fig. 4 Temperature dependence of the Seebeck coefficients of $La_{0.1}Y_xSr_{0.9-x}TiO_3$ ($x = 0.01$, 0.03, 0.05, 0.08, and 0.10) ceramics

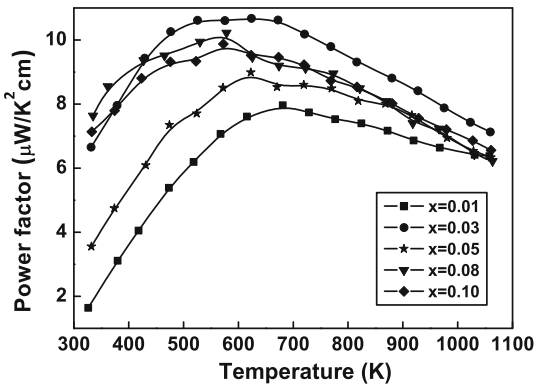

Fig. 5 Temperature dependence of the power factor of $La_{0.1}Y_xSr_{0.9-x}TiO_3$ ($x = 0.01$, 0.03, 0.05, 0.08, and 0.10) ceramics

samples are 8.0 at 681 K, 11 at 624 K, 9.0 at 623 K, 10 at 578 K, and 9.9 μW cm^{-1} K^{-2} at 572 K, respectively. Ceramic sample of $La_{0.1}Y_{0.03}Sr_{0.87}TiO_3$ exhibits the highest value of power factor, and the value almost stay put (all above 11 μW cm^{-1} K^{-2}) in the temperature range of 500 to 700 K. This result may benefit for practical applications of thermoelectric ceramics.

Conclusion

Influence of Y doping effect on $La_{0.1}Sr_{0.9}TiO_3$ has been studied from samples prepared by the conventional solid state reaction method. The major phase of all samples is cubic perovskite structure, with a second phase ($Y_2Ti_2O_7$) is identified in samples for $x = 0.05$, 0.08, and 0.10. The electrical resistivity decreases with increasing of yttrium concentration, the lowest electrical resistivity is obtained as 0.8 mΩ cm for $x = 0.10$ sample at 333 K. The sample of $x = 0.03$ possesses the highest absolute Seebeck coefficient in high temperature range, and exhibits the highest power factor as 11 μW cm^{-1} K^{-2} at 624 K.

Acknowledgements The study is financially supported National Basic Research Program of China of 2007CB607504, Natural Science Fund of China under Grant nos. 50902086 and 50572052, Shandong Province Natural Science Foundation under Grant nos. ZR2009AQ003 and Graduate Independent Innovation Foundation of Shandong University under Grant no. yzc09076.

References

1. Sootsman JR, Chung DY, Kanatzidis MG (2009) Angew Chem Int Ed 48:8616
2. Terasaki I, Sasago Y, Uchinokura K (1997) Phys Rev B 56:12685. doi:10.1103/PhysRevB.56.R12685
3. Funahashi R, Matsubara I, Ikuta H et al (2000) Jpn J Appl Phys 39:L1127
4. Okuda T, Nakanishi K, Miyasaka S et al (2001) Phys Rev B 63:113104. doi:10.1103/PhysRevB.63.113104
5. Miyazaki Y, Miura T, Ono Y et al (2002) Jpn J Appl Phys 41:L849
6. Muta H, Kurosaki K, Yamanaka S (2003) J Alloy Compd 350:292. doi:10.1016/S0925-8388(02)00972-6
7. Obara H, Yamamoto A, Lee CH et al (2004) Jpn J Appl Phys 43:L540. doi:10.1143/jjap.43.l540
8. Muta H, Kurosaki K, Yamanaka S (2005) J Alloy Compd 392:306. doi:10.1016/j.jallcom.2004.09.005
9. Ohta S, Nomura T, Ohta H et al (2005) Appl Phys Lett 87:092108. doi:10.1063/1.2035889
10. Liu HQ, Zhao XB, Liu F et al (2008) J Mater Sci 43:6933. doi:10.1007/s10853-008-2990-6
11. Wang HC, Wang CL, Zhang JL et al (2010) Curr Appl Phys 10:866. doi:10.1016/j.cap.2009.10.009
12. Wang HC, Wang CL, Su WB et al (2010) Mater Res Bull 45:809. doi:10.1016/j.materresbull.2010.03.018
13. Shang PP, Zhang BP, Li JF et al (2010) Solid State Sci 12:1341. doi:10.1016/j.solidstatesciences.2010.05.005
14. Jalan B, Stemmer S (2010) Appl Phys Lett 97:042106. doi:04210610.1063/1.3471398
15. Hui SQ, Petric A (2002) J Electrochem Soc 149:J1. doi:10.1149/1.1420706